Half-lives of trinuclear molecules

F. Carstoiu,[1,2,*] I. Bulboacă,[1] A. Săndulescu,[1,2] and W. Greiner[2]
[1]*National Institute of Nuclear Physics and Engineering, P.O. Box MG-6, 76900 Bucharest-Magurele, Romania*
[2]*Institut für Theoretische Physik der J. W. Goethe Universität, D-60054, Frankfurt am Main, Germany*
(Received 26 October 1999; published 10 March 2000)

Recent discoveries of ^{10}Be and ^{12}C accompanied cold fission in the spontaneous fission of ^{252}Cf lead to the surprising result that long living trinuclear molecules may exists. For the description of the dynamics and decay of such molecules, we used a coplanar three body cluster model (two deformed fragments and an α particle) with a three body potential computed by a double folding potential generated by M3Y effective interaction. A repulsive compression term was included. The computed α ternary cold fission yields are in agreement with the experiment. The energy and angular distributions of the three clusters at infinity and the half-lives are strongly dependent of the initial positions of the α particle relative to the two fragments and of mass asymmetry of the fragments. The evaluated lifetimes of such trinuclear molecules are quite large, of the order of one second.

PACS number(s): 25.85.Ca, 21.60.Gx, 23.70.+j

I. INTRODUCTION

Cluster radioactivity [1], cold binary fission [2,3], cold ternary fission [4–6], and cold fusion [7,8] are well established phenomena. These processes were predicted based on the idea that cold rearrangement of large groups of nucleons is possible [7]. The recent direct evidence of cold ^{4}He [4], ^{10}Be [5], and ^{12}C [9] ternary yields was possible mainly due to the development of large Ge-detector arrays such as Gammasphere and Euroball. By using especially multiple γ-coincidence technique the correlations between the two heavy fragments and the light particle were observed unambiguously. In the case of ^{10}Be cold ternary spontaneous fission of ^{252}Cf only the triple γ-coincidence was used. The γ-ray corresponding to the decay of the first 2^{+} state in ^{10}Be was detected in coincidence with the γ rays of the fission partners ^{96}Sr and ^{146}Ba. The yield of such a ternary cold splitting is of the order of 4×10^{-4} per 100 fission events. The surprising result is that the γ transition in ^{10}Be is not Doppler broadened as one would expect if the system separates immediately into three clusters and ^{10}Be decays in flight. The other key experimental fact is that the γ ray seems to be 6 KeV lower in energy than expected from the compilation [10]. The energy of the first excited state in ^{10}Be was remeasured recently with a high precision in a ^{9}Be$(d,p\gamma)^{10}$Be reaction [11] and was found to be in excellent agreement with the literature value. The only possible interpretation is the existence of a long living nuclear molecule where the three nuclei stick together with a half-life larger than 10^{-12} s [5]. Recently, this result was confirmed by the discovery of ^{12}C cold ternary fragmentation in the spontaneous fission of ^{252}Cf [9]. Again only the triple γ correlations between the first two transitions in ^{12}C at 3214.8 and 4438.0 KeV and the first excited state in the light (^{81}Ge-^{159}Nd) or heavy (^{147}La-^{93}Br) fragment were observed. No excited states were observed in the other fragment. It was shown that the γ transitions are not Doppler broadened, confirming again the existence of such long living molecules. Evidently, the inclusion in the future experiments of fragment and light charge detectors will provide a complete set of data necessary to clarify the existence of such long living molecules.

In this paper we describe a dynamical three cluster model appropriate for the evaluation of a cold ternary fission process at a quantitative level. Initial configurations, dynamical trajectories in the classically forbidden region, penetrabilities, trajectories of the fragments in the asymptotic region, angular, and energy distributions of the decaying fragments are deduced from a three body interaction potential. We obtain a set of coupled differential equations which satisfy the minimum action principle, appropriate for the description of the trajectories under the barrier. We show that to the lowest order of the WKB approximation there are no penetration solutions for a multidimensional case. We show how to circumvent this difficulty by solving the steepest descent equations near the turning points. By solving dynamical equations we deduce trajectories, barriers, penetrabilities, relative production yields, angular, and energy distributions for the decaying fragments. From the calculated penetrabilities and the barrier assault frequency we estimate the lifetimes for the giant trinuclear molecules.

The paper is organized as follows. Section II deals with a brief description of our reaction model, results from numerical calculations are presented in Sec. III, and we end up with some conclusions.

II. THE REACTION MODEL

About 90% of the light particles emitted in the ternary spontaneous fission are α particles. That prompted us to study the cold (neutronless) α ternary fission of ^{252}Cf. A coplanar three cluster model consisting of two deformed fragments and a spherical α particle was considered. The kinematics of the problem is described in detail in our paper [12]. Three main coordinates were retained for the description of the dynamics during the rearrangement and penetra-

*Electronic address: carstoiu@theor1.theory.nipne.ro

tion through the barrier processes. These are (x_α, y_α), the coordinates of the c.m. of the α particle, and a collective coordinate R describing the separation distance between the heavy fragments along the fission axis. Center-of-mass correlations are fully taken into account in all calculations. We assume that the fission axis is conserved during the penetration process. As a consequence, the total energy is only approximately conserved, but this approximation has little influence on the calculated penetrabilities. No preformation factors were included in our description. Our previous study of cold (neutronless) binary fission of ^{252}Cf showed clearly that the inclusion of high rank deformations into calculation is necessary in order to obtain a correct description of the cold binary yields [3]. Consequently, we included realistic deformations for the description of the fragment shapes. The three body potential was computed with the help of a double folding potential generated by M3Y-*NN* effective interaction [13]. We would like to stress that the interaction barriers are calculated quite accurately on the absolute scale and that the touching configuration for the heavy fragments is situated outside the barrier. Due to the lack of any explicit density dependence in the M3Y effective interaction, which leads to unphysically deep potentials for large density overlaps, in the following we introduce a compression term in order to correct the short range dependence of the calculated interaction potentials which read

$$V(\vec{R}) = \int d\vec{r}_1 d\vec{r}_2 \rho_1(\vec{r}_1)\rho_2(\vec{r}_2) v(|\vec{s}|) + V_{\text{comp0}} \int d\vec{r}_1 d\vec{r}_2 \tilde{\rho}_1(\vec{r}_1)\tilde{\rho}_2(\vec{r}_2)\delta(\vec{s}), \qquad (1)$$

where $v(|\vec{s}|)$ is the effective interaction (depending on the separation distance of the interacting nucleons $\vec{s} = \vec{r}_1 + \vec{R} - \vec{r}_2$) which includes the usual pseudo-δ knock-on exchange term [14], $\rho_i(\vec{r}_i)$, $i = 1,2$ are the ground state one body densities taken as deformed two parameter Fermi distributions in the intrinsic frames, $\tilde{\rho}_i(\vec{r}_i) i = 1,2$ are the corresponding sharp fragment densities with R_{sharp} given by the equation $\langle r^2 \rangle = 3/5 R^2_{\text{sharp}}$ and V_{comp0} is the strength of the compression term. With the above definition, the compression term gives rise to a repulsive component in the interaction potential which is proportional to the volume overlap of the two densities. It is short ranged and contributes to the integral (1) only for $|r_1 - r_2| \leqslant R \leqslant r_1 + r_2$ and therefore the interaction potential is unaltered beyond the touching configuration $R \geqslant R_{\text{touch}} = R_1 + R_2$. For the α particle we used a harmonic oscillator density with a width parameter $\beta^2 = 0.47$ fm^{-2}. The Coulomb component was calculated also by double folding using appropriate charge densities. In evaluating the integrals in Eq. (1) we used a multipole expansion of the one body densities which allows for the inclusion of the deformation to all orders and arbitrary orientation of the nuclei [15]. The strength of the compression term is largely uncertain. In principle it should be determined from EOS at twice the normal density of nuclear matter. Throughout the paper we have used a value $V_{\text{comp0}} = 300$ MeV, close to the value used by Uegaki [16] for molecular resonances in medium-weight nuclei. Other details on the computational techniques used for the evaluation of folding integrals in Eq. (1) and the axial static deformations are given in Ref. [12]. The role played by high order static deformations is illustrated in Fig. 1 for the channel ^{92}Kr+^{156}Nd. The fragments were chosen with aligned symmetry axes. When only the monopole terms are allowed (terms coupling to a total angular momentum $\lambda_3 = 0$), the interaction potential is dominated by the compression and Coulomb terms (dotted line). If higher multipole are included, a typical quasimolecular pattern emerges (dash-dotted and continuous lines). Clearly, the height and the maximum barrier are controlled by high order multipoles. One see also that the barrier is situated outside the touching configuration and essentially the barrier region involves density overlaps significantly less than the nuclear matter saturation density.

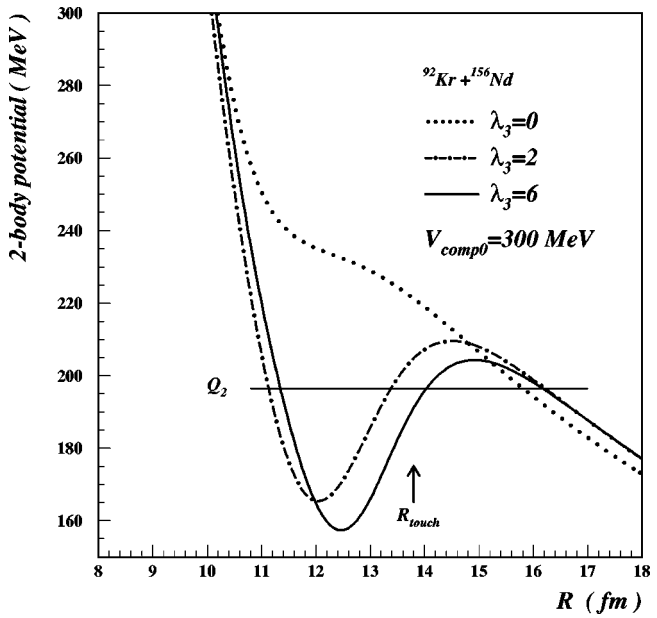

FIG. 1. Interaction potential between the heavy fragments ^{92}Kr+^{156}Nd for a nose to nose configuration calculated with a compression strength of $V_{\text{comp0}} = 300$ MeV. Deformation parameters are taken from Ref. [18]. The dotted line calculation includes all the terms in the multipole expansion coupled to a total angular momentum $\lambda_3 = 0$. Dash-dotted line includes terms up to $\lambda_3 = 2$ and continuous line includes terms up to $\lambda_3 = 6$. The interfragment distance for the touching configuration is indicated by an arrow. The horizontal line indicates the Q value for the reaction ^{248}Cm$\rightarrow^{92}$Kr $+^{156}$Nd.

We would like to mention that the introduction of the compression term greatly improves the short range dependence of the interaction potential. The three body potential assumed to be the sum of all two body components displays a quasimolecular pattern with two minima in the equatorial region and two polar minima. The situation is illustrated in Fig. 2 for the fragmentation channel ^{252}Cf$\rightarrow\alpha+^{92}$Kr $+^{156}$Nd and for an interfragment distance $R = 15$ fm. The minima in the equatorial region are equivalent due to axial symmetry. The potentials for nose to nose configurations in each two body channel are displayed in Fig. 3 (upper panel).

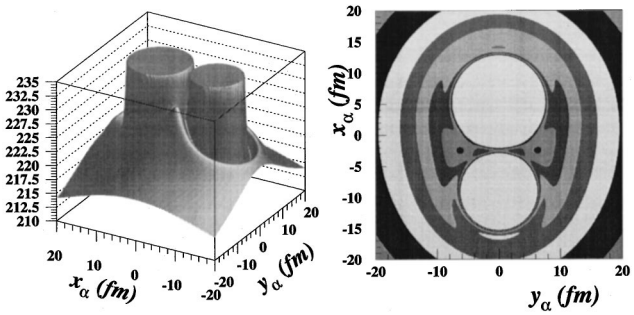

FIG. 2. Left panel: the three dimensional plot of the interaction potential for the splitting $^{252}\mathrm{Cf}\rightarrow\alpha+^{92}\mathrm{Kr}+^{156}\mathrm{Nd}$ at interfragment distance $R=15$ fm. Right panel: x-y projection of the same potential.

The minima in the α particle components are situated at 7 and 8.5 fm with respect to the light and heavy fragment, respectively, which means that quasistable configurations are formed in the three body system with the α particle situated at rather large distances. We also mention that quasistable configurations are formed if and only if a molecular pattern is obtained in all two body channels. If the minimum in one two body channel disappears (e.g., in the α-light fragment channel), then the minimum in the three body potential is attained with the α particle situated at infinity (with respect to that fragment) and the stability is lost. This is in contrast with the situation in light Borromean nuclei (e.g., ^{6}He and ^{11}Li) where a bound three body state close to the threshold is formed (the Efimov quantum effect) while all two body channels are unbounded. This is due to the fact that we are treating classically the interaction.

Our strategy is clear now. We assume first that the movement of the three particles is so slow that the system adjusts adiabatically to stay in a configuration corresponding to the minimum in the three body potential. The corresponding barrier and the α particle trajectory are displayed in Fig. 3 (middle and bottom panels) with continuous lines. Also the total available reaction energy is indicated (Q_3). We distinguish three regions: the minimum where the system oscillates corresponding to a cold rearrangement process, the classically forbidden region (the barrier), and the asymptotic region (beyond the outer turning point) where the system decays into three fragments. In the minimum region we solved the classical equations of motion thus obtaining the oscillation time T_{osc}, the corresponding α particle trajectory and the inner turning point. The oscillation time is of the order of 0.6×10^{-21} s and the barrier assault frequency of the order $\nu\sim1.7\times10^{21}$ s^{-1}. The zero point energy is estimated from the uncertainty principle giving $E_0\simeq0.9$ MeV for highly deformed fragments and slightly larger for spherical splittings ($\sim$1.2 MeV). In the classically forbidden region we solve the semiclassical trajectory equations for the relevant degrees of freedom [12]. For completeness we write them here in a simpler but equivalent form

$$x_i''=\frac{M}{2(Q-V)}\left(\frac{x_i'}{m_1}\frac{\partial V}{\partial x_1}-\frac{1}{m_i}\frac{\partial V}{\partial x_i}\right), \qquad (2)$$

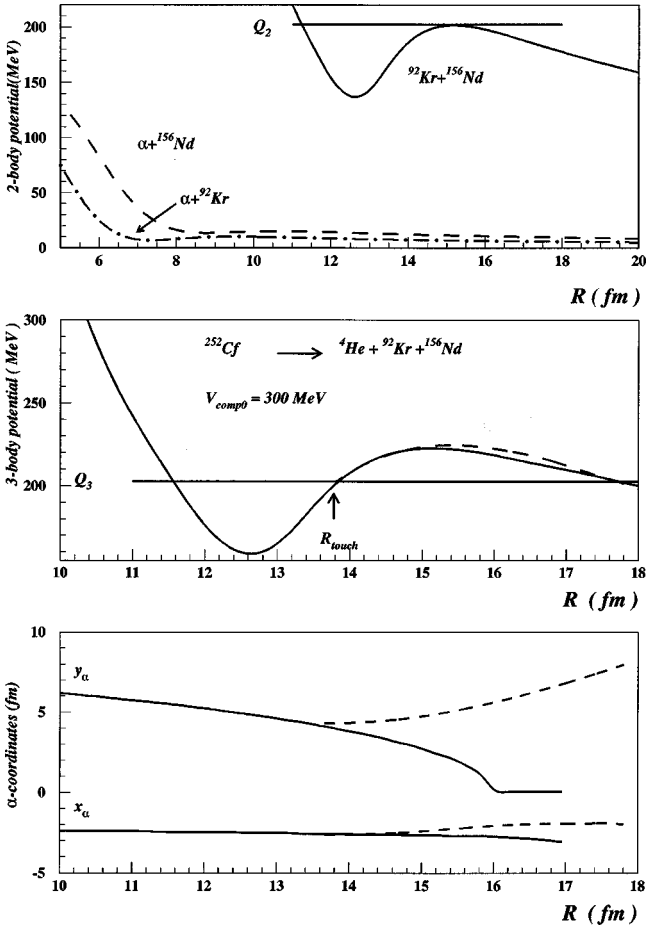

FIG. 3. The two body components of the interaction potential calculated with a compression strength $V_{\mathrm{comp0}}=300$ MeV are displayed in the upper panel. The adiabatic (continuous line) and dynamic (dashed line) barrier (see text for details) are given in the middle panel. The corresponding adiabatic (continuous line) and dynamic (dashed line) α particle trajectories are given in the bottom panel. The fragmentation channel is indicated on the figure.

with $M=m_1+\Sigma m_j(x_j')^2$ the effective mass (or the effective inertia) and $x'=dx/dx_1$. m_i are the masses for the corresponding degrees of freedom, Q is the reaction energy. Mixed derivatives do not appear in the effective inertia since in our case the mass tensor is diagonal. x_1 is one of the relevant variables (supposed to vary monotonically) chosen to parametrize the trajectory. In practice we found that the variable R is the best candidate. The coupled differential equations (2) describe the motion of the system in the barrier region and satisfy the minimum action principle. It can be shown that the set of equations (2) is fully equivalent with the classical equations of motion in imaginary time $\tau=it$. The reduced action is given by

$$S_0=\int\sqrt{2(V-Q)\left[m_1+\sum_i m_i\left(\frac{dx_i}{dx_1}\right)^2\right]}dx_1, \qquad (3)$$

and the penetrability factor is simply $P=e^{-2S_0/\hbar}$. A close examination of Eq. (2) shows that the semiclassical approximation is not valid on the surface $Q=V$. In order to have a

solution we must require that the factor in parenthesis in Eq. (2) vanishes on that surface. This gives us the so-called *transversality conditions* or the *steepest descent equations* [17]

$$\frac{m_i x_i'}{\partial V/\partial x_i} = \frac{m_1}{\partial V/\partial x_1}, \tag{4}$$

which are solved near the turning points. One extremely important problem relates to the existence of penetrating solutions for Eq. (2). While such a question does not appear in the one-dimensional case, in the multidimensional case the answer is not obvious. Consider, for example, the following analytical case. Take the many body potential in the form $V=V_0-\Sigma\alpha_i x_i^2$ with V_0 an arbitrary constant. The solutions for this potential (in the imaginary time τ) for given initial conditions x_{i0}, are $x_i=x_{i0}\cos(\omega_i\tau)$, $\omega_i=\sqrt{2\alpha_i/m_i}$. The exit conditions $dx_i/d\tau=0$, $i\geqslant 1$, require $\sin(\omega_i\tau_f)=0\Rightarrow\omega_i$ must be in ratios of rational numbers, a condition hardly satisfied for any realistic problem. Therefore, in the semiclassical approximation the trajectory is localized inside the barrier, oscillating indefinitely between the turning points. We circumvent this difficulty by determining explicitly the regions where the semiclassical approximation (WKB) is valid (usually in the middle of the barrier) and solving the steepest descent equations in the region of the turning points. Note that the WKB approximation requires that

$$\left|\sum_i \frac{\hbar}{m_i}\frac{\partial^2 S_0}{\partial x_i^2}\right| \ll \left|\sum_i \frac{1}{m_i}\left(\frac{\partial S_0}{\partial x_i}\right)^2\right|, \tag{5}$$

which can be transformed to

$$\left|\hbar\sum_i \frac{\partial V}{\partial x_i}\frac{1}{m_i\dot{x}_i}\right| \ll \left|\sum_i m_i\dot{x}_i^2\right|. \tag{6}$$

The last inequality (with $\dot{x}=dx/d\tau$) is valid also in the barrier region. Near the turning points ($V=Q$) the condition (6) is not satisfied since $\dot{x}_i\approx 0$. In practice we evaluated Eq. (6) along the trajectory and near the turning points we switched automatically to solving Eq. (4). Usually the portion of the trajectory obtained with Eq. (4) gives little contribution to the total action. When this contribution becomes important one changes the initial conditions for integrating Eq. (2).

III. RESULTS

An example of dynamical barrier and α particle trajectory is given in Fig. 3 (middle and bottom panels) with dashed lines. The dynamical trajectory should be contrasted with the adiabatic (static) one. In the dynamical case the α particle gets away from the interfragment axis with large y_α values at the outer turning point. Contrary, in the adiabatic case the α particle gets closer to the interfragment axis up to $y_\alpha\sim 0$. We mention that for the example given in Fig. 3 the minimum in the three body potential disappears at a distance of the order of $\sim$17 fm and the adiabatic barrier and trajectory are no longer well defined.

Having solved the dynamical equations of motion, using the reaction energies (Q_3) calculated from the experimental masses or in few cases taken from the theoretical predictions of Möller and Nix [18] we evaluate the penetrabilities as described above. The relative production yields are evaluated from the simple formula

$$Y_L(A_L,Z_L)=\frac{P_L(A_L,Z_L)}{\sum_{L'} P_{L'}(A_{L'},Z_{L'})}. \tag{7}$$

Evidently we assume that the preformation factors are the same for all cold splittings and consequently in the expression (7) this factor cancels. The calculated yields (normalized to the experimental ones [4]) are displayed in Fig. 4. Full details of the calculation are given in Table I. This includes the 16 splittings we have considered in this paper, the interfragment distance for touching configuration (R_{touch}), the maximum of the dynamical barrier ($B_{\max}$) and the reaction energy (Q_3), the initial configuration at the inner turning point ($R_i, x_{\alpha i}, y_{\alpha i}$), the final configuration at the outer turning point ($R_f, x_{\alpha f}, y_{\alpha f}$), the dynamic penetrability (P), the final kinetic α particle energy (E_α), and the scattering angle (θ_α). We define the mass asymmetry as $\eta=(A_H$

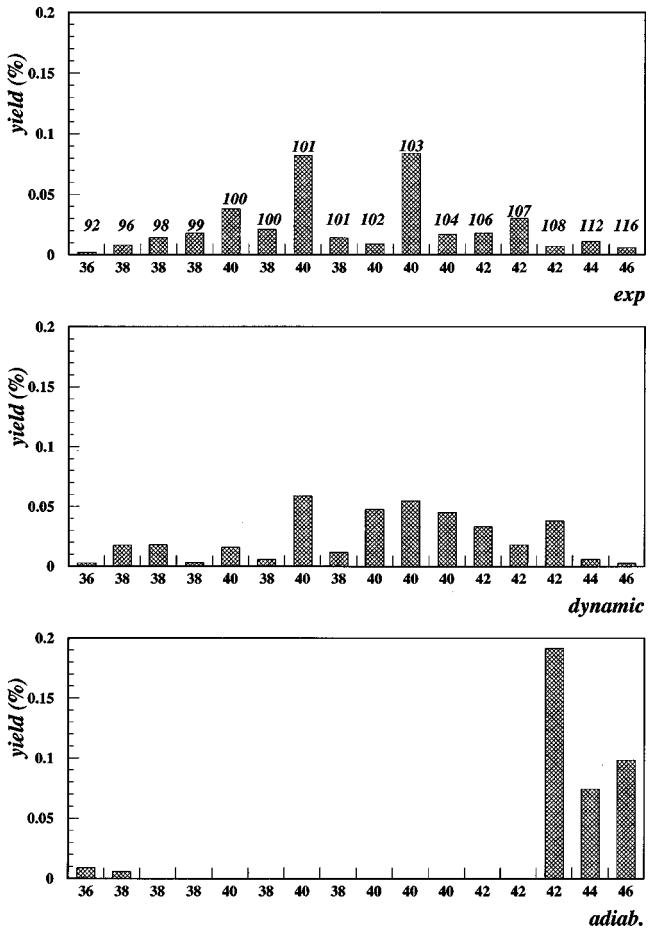

FIG. 4. Comparison of experimental yields [4] (upper panel) with the dynamic (middle) and adiabatic (bottom) results. The fragmentation channel is indicated by the charge number (on the x axis) and by the mass number (on top of the stacks) of the light fragment.

TABLE I. Results for the tunneling trajectories in the WKB approximation for 16 fragmentation channels: touching configuration, barrier maximum, initial and final configurations on the penetration path, the penetrability factor, energy and scattering angle for the α particle. The coordinates of the α particle are given in the c.m. of the three body system.

L	H	R_{touch} [fm]	$B_{\max}$ [MeV]	Q_3 [MeV]	R_i [fm]	$x_{\alpha i}$ [fm]	$y_{\alpha i}$ [fm]	R_f [fm]	$x_{\alpha f}$ [fm]	$y_{\alpha f}$ [fm]	P 10^{-21}	E_α [MeV]	θ_α [deg]
$^{92}_{36}$Kr	$^{156}_{60}$Nd	13.78	222.7	202.7	13.85	−2.54	3.95	17.8	−0.47	7.5	0.31	21.1	−75.9
$^{96}_{38}$Sr	$^{152}_{58}$Ce	14.02	224.4	205.8	14.02	−2.20	3.90	17.9	−1.97	8.1	1.91	19.0	−80.4
$^{98}_{38}$Sr	$^{152}_{58}$Ce	14.12	224.4	205.2	14.07	−1.95	3.86	17.9	−1.46	7.9	1.92	19.6	−79.6
$^{99}_{38}$Sr	$^{149}_{58}$Ce	14.39	222.5	202.5	14.32	−1.95	3.85	18.3	−1.64	7.6	0.32	19.6	−79.7
$^{100}_{40}$Zr	$^{148}_{56}$Ba	14.15	227.7	208.2	14.11	−1.82	3.85	17.9	−1.64	7.8	1.73	19.4	−82.0
$^{100}_{38}$Sr	$^{148}_{58}$Ce	14.16	223.9	204.2	14.16	−1.80	3.85	18.1	−1.70	7.8	0.64	19.4	−80.1
$^{101}_{40}$Zr	$^{147}_{56}$Ba	14.33	227.5	208.5	14.17	−1.70	3.80	17.9	−1.52	7.7	6.29	19.6	−81.9
$^{101}_{38}$Sr	$^{147}_{58}$Ce	14.92	220.4	201.2	14.55	−1.90	3.74	18.5	−0.86	7.1	1.26	20.4	−77.9
$^{102}_{40}$Zr	$^{146}_{56}$Ba	14.13	229.5	210.4	13.93	−1.60	3.90	17.7	−1.75	8.2	5.11	19.2	−82.6
$^{103}_{40}$Zr	$^{145}_{56}$Ba	14.25	228.9	210.0	14.00	−1.55	3.85	17.8	−1.18	7.7	5.91	19.7	−81.7
$^{104}_{40}$Zr	$^{144}_{56}$Ba	13.96	230.8	211.7	13.80	−1.50	3.92	17.5	−1.43	8.2	4.86	19.2	−82.4
$^{106}_{42}$Mo	$^{142}_{54}$Xe	13.78	234.7	215.3	13.67	−1.20	4.04	17.4	−1.61	8.5	3.56	18.9	−84.8
$^{107}_{42}$Mo	$^{141}_{54}$Xe	13.79	234.5	214.9	13.69	−1.10	4.06	17.4	−1.61	8.5	1.92	18.9	−84.9
$^{108}_{42}$Mo	$^{140}_{54}$Xe	13.29	236.9	217.8	13.40	−1.00	4.26	17.1	−1.61	8.8	4.11	18.6	−84.9
$^{112}_{44}$Ru	$^{136}_{52}$Te	12.75	244.1	223.9	12.90	−0.70	4.43	16.6	−1.45	9.3	0.62	18.2	−86.8
$^{116}_{46}$Pd	$^{132}_{50}$Sn	12.31	250.8	230.2	12.35	−0.45	4.71	16.0	−1.28	9.8	0.24	17.8	−88.4

$-A_L)/248$. For the splittings given in Table I, η varies between 0.26 and 0.06. From the table it is evident that the penetration process starts always in a configuration with $R_i \simeq R_{\text{touch}}$. Along the sequence of splittings we considered in Table I, the reaction energy (Q_3) varies by more than 28 MeV and though the dynamic penetrability is very stable. This is due to the fact that along the dynamic trajectory the action is minimal for given initial conditions, i.e., on the trajectory the resistance (effective inertia) to a change in the α-particle coordinates is minimal. As a consequence, the mass distribution is rather flat, showing nonvanishing and comparable mass yields for a large range of mass asymmetry in agreement with the experiment. Another remark concerns the energy and the scattering angle of the α particle. The energy is larger for large asymmetry mass splittings and the scattering angle is smaller. The average values, taking the calculated dynamical yields as weighting factors are $\langle E_{kL}\rangle = 111.0 \pm 1.3$ MeV, $\langle E_{kH}\rangle = 80.6 \pm 4.5$ MeV, $\langle E_{k\alpha}\rangle = 19.3 \pm 0.5$ MeV, and $\langle \theta_\alpha \rangle = -82.5 \pm 1.9°$. The quoted variances are calculated from the width distributions given in Table I. We shall show below that these variances become much larger if quantum fluctuations are taken into account. According to Heeg [19], the mean experimental angle, measured with respect to the fission axis oriented towards the light fragment (opposite to our convention, see below) is 83°. The adiabatic scenario gives ternary yields only for splittings with one of the fragments spherical, as we have shown in our previous paper [12]. The corresponding yields are evidently dominated by Q-value effects. Only high Q-value channels contribute to the total yield. In the dynamical calculation there is a delicate interplay between deformation, Q-value, and penetration path effects. Note that the theoretical yields are calculated strictly at zero excitation energy and we neglected the level density close to the ground state of the fragments and as a result the odd-even effects, noticeable in the experiment around the masses $A_L = 101$, 103, 107 are not well reproduced.

We evaluate the lifetime for the decaying molecule using the relation $T_{1/2} = \ln 2/\nu P$, where ν is the barrier assault frequency and P the penetrability.

Next we consider fluctuations in the entrance point since the calculated action along the penetration path should be minimized not only with respect to the path, but also with respect to the initial conditions. If we neglect the α particle coordinates, then the lowest quasimolecular state of the system in the potential minimum is of the form $\Psi \sim \exp[-\frac{1}{2}\alpha(R-R_0)^2]$. From the estimated energy for the lowest state we have $E_0 = \hbar^2\alpha/2m$ and the estimated value for the distribution width is $1/2\sqrt{\alpha} = 0.7$ fm. Therefore we started a Monte Carlo evaluation of the trajectories using as inner turning point $R_i = R_{t1} + \sigma \times \text{Gauss(seed)}$ where R_{t1} is the turning point given by the minimization procedure, Gauss-(seed) is a random Gaussian generator with zero mean value and variance 1. σ is the desired variance of the generated distribution, taken here of the order of 0.1 fm, a rather conservative value. For all generated R_i values we search for the solutions of the equation for energy conservation $V[R_i, x_\alpha(R_i), y_\alpha(R_i)] = Q_3$ at the entrance point. In practice, we relaxed this condition, searching for solutions $(x_{\alpha i}, y_{\alpha i})$ in a band $Q_3 \pm 50$ KeV. No initial velocity distributions were considered in this simulation, since in our particular system of coordinates it is difficult to conserve the total linear momentum. In this way a number of some 8000 initial positions were generated. The calculation was completed by solving the dynamical equations in the barrier up to the outer turning

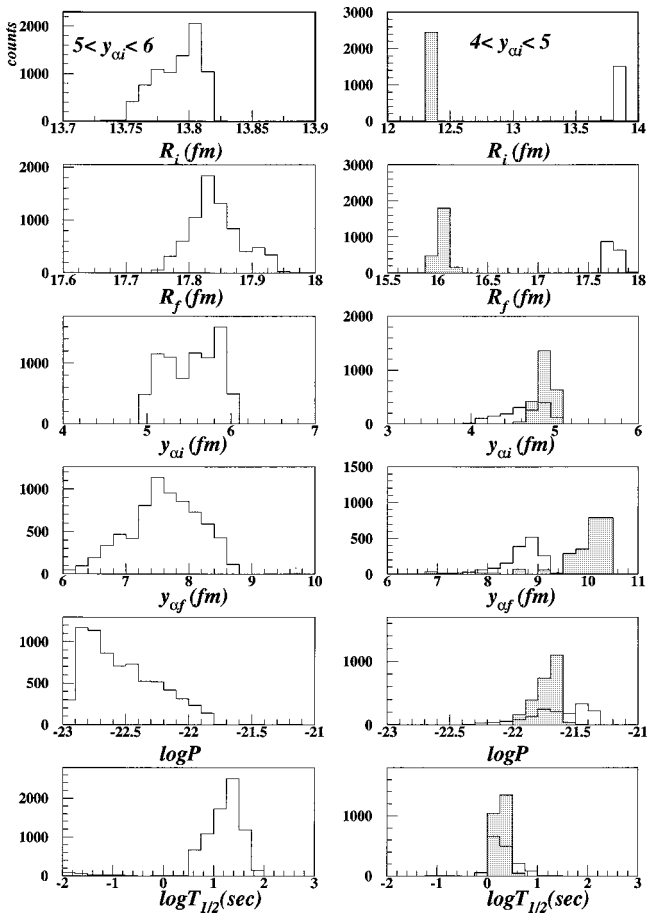

FIG. 5. Initial and final distributions for dynamic variables obtained in a Monte Carlo simulation. Left panels include selected events in the band $5 \leqslant y_{\alpha i} \leqslant 6$ fm; right panels are for events in the band $4 \leqslant y_{\alpha i} \leqslant 5$ fm. The last two rows are for the distribution of the decimal logarithm of the penetrability (P) and for the half-lives ($T_{1/2}$). Filled histograms are for the splitting $^{252}\mathrm{Cf} \rightarrow {}^{4}\mathrm{He} + {}^{116}\mathrm{Pd} + {}^{132}\mathrm{Sn}$. The other histograms are for the splitting $^{252}\mathrm{Cf} \rightarrow {}^{4}\mathrm{He} + {}^{92}\mathrm{Kr} + {}^{156}\mathrm{Nd}$.

point. From then on the system disintegrates. The final energy and angular distribution of the fragments were obtained by solving the classical equation of motion for a three body system. Since the exit point locates at rather large distances ($R_f \sim 18$ fm) and $y_{\alpha f} \sim 8$ fm, the nuclear forces are completely negligible, and we used only the monopole-monopole part of the Coulomb interaction. We have shown [20] that quadrupole-monopole and other higher multipolarity terms have little influence on the final distributions. The results of the simulations are displayed in Figs. 5 and 6 for the splitting $^{252}\mathrm{Cf} \rightarrow \alpha + {}^{92}\mathrm{Kr} + {}^{156}\mathrm{Nd}$ ($\eta = 0.26$). We have also considered the more symmetric splitting $^{252}\mathrm{Cf} \rightarrow \alpha + {}^{116}\mathrm{Pd} + {}^{132}\mathrm{Sn}$ ($\eta = 0.06$) shown by shadowed histograms in Figs. 5 and 6. In left panels we have selected all events in the band $5 \leqslant y_{\alpha i} \leqslant 6$ fm and $4 \leqslant y_{\alpha i} \leqslant 5$ fm in the right panels. Much lower initial values $y_{\alpha i}$ correspond to an α particle in overlap with the fragments and lead to trajectories traversing one of the heavy fragments and with penetrabilities of the order 10^{-100} or smaller and they are disregarded. The higher the initial position of the α particle, the wider the distribution in

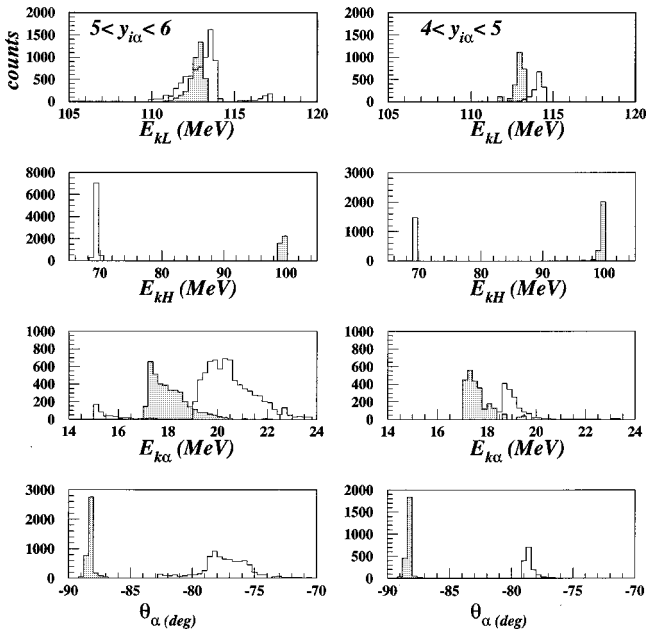

FIG. 6. Energy distributions for the decaying light (L), heavy (H), and alpha (α) particle. Angular distribution (θ_α) is given in the last row. See caption to the Fig. 5.

the final $y_{\alpha f}$ coordinate. Also the energy distribution of the light fragment (E_{kL}) is wider. The mean kinetic energy for the α particle is 21(18) MeV and the mean scattering angle is $-78°$ ($-88°$) for large (small) η. The angle is negative since we have chosen a system of coordinates with the light fragment placed on the left side, and the α particle is deviated strongly by the heavy fragment, so the scattering angle is always in the second quadrant ($\theta_\alpha \geqslant \pi/2$). A typical trajec-

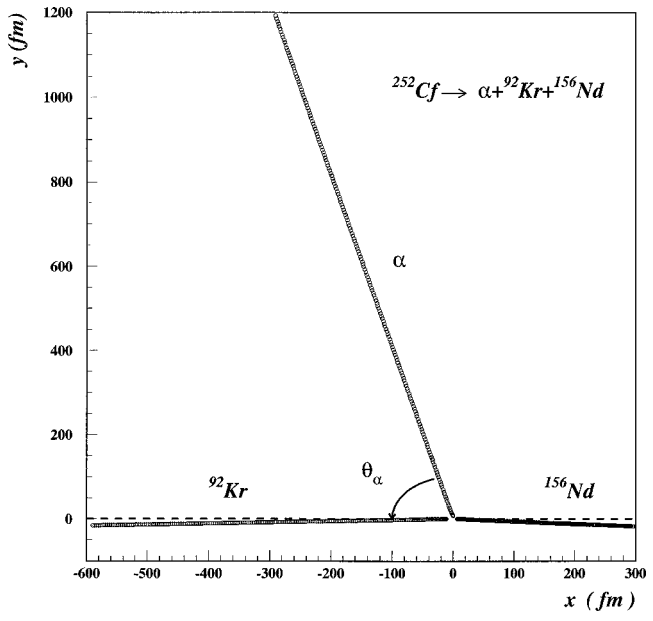

FIG. 7. Typical trajectory calculation (including only monopole-monopole Coulomb terms) for the decay of a three body system. The recoil of heavy fragments in the presence of the α particle is small but sizable. The scattering angle is defined on the figure.

tory calculation is illustrated in Fig. 7. For initial positions in the lower band (right panels in Figs. 5 and 6) all distributions are much narrower, showing a strong focusing effect. The final kinetic energy $E_{k\alpha}$ lowers to 19(17.5) MeV and the scattering angle is $-79°$ $(-88°)$. In the upper position band the penetrabilities are small $(\leqslant 10^{-22})$ and the lifetime is of the order of tens of seconds. In the lower band the penetrabilities increase (10^{-21}) and the lifetime varies between 1 and 10 s. As we must minimize the reduced action, one should choose the trajectory with maximum of penetrability. Therefore our model predicts lifetimes for the trinuclear molecule of the order of 1 s. Of course, all distributions will be much larger if averaged over all fragmentation channels. Note the strong dependence of all distributions on the mass asymmetry of the heavy fragments (and implicitly on Q value and deformation) (Figs. 5 and 6). This is especially evident for exit configuration $(R_f, y_{\alpha f})$ and for the kinematic variables of the fragments $(E_{k\alpha}, E_{kH}, \theta_\alpha)$.

IV. CONCLUSIONS

In conclusion we designed a coplanar three cluster model which describes reasonably well the cold ternary spontaneous fission process from the early stage of cold rearrangement of nucleons in the potential minimum, to the last stage of the decaying nuclear molecule in the asymptotic region. The complicated penetration process in a multidimensional barrier was described dynamically by solving a set of semiclassical coupled differential equations which satisfies the minimum principle action. Minimum action with respect to the initial conditions was found in an extensive Monte Carlo calculation. The asymptotic distributions of kinematical variables were obtained by solving the classical equations of motion for the three fragments. The three body interaction potential was generated from a *G*-matrix density independent effective interaction in a double folding procedure. The short range behavior of the interacting potential is greatly improved by introducing a compression term which suppresses large density overlaps. The obtained three body potential shows a typical quasimolecular pattern and relatively stable configurations are predicted with the α particle laying at rather large distances from the heavy fragments. The lifetime predicted by the model is of the order of 1 s. The model could be tested experimentally since the final energy and angular distributions of the decaying fragments are strongly correlated with the initial configurations prior to the penetration process and with the mass asymmetry of the fragments. The model could be improved by increasing the number of relevant degrees of freedom (e.g., by including a relative coordinate in the y direction for the heavy fragments and allowing for collective rotations).

ACKNOWLEDGMENTS

The authors are grateful to Professor G. Münzenberg for fruitful discussions.

[1] A. Sandulescu and W. Greiner, Rep. Prog. Phys. **55**, 1423 (1992).
[2] A. Sandulescu, A. Florescu, F. Carstoiu, W. Greiner, J. H. Hamilton, A. V. Ramayya, and B. R. S. Babu, Phys. Rev. C **54**, 258 (1996).
[3] A. Sandulescu, S. Misicu, F. Carstoiu, A. Florescu, and W. Greiner, Phys. Rev. C **57**, 2321 (1998).
[4] A. V. Ramayya, J. H. Hamilton, J. K. Hwang, L. K. Peker, J. Kormicki, B. R. S. Babu, T. N. Ginter, A. Sandulescu, A. Florescu, F. Carstoiu, W. Greiner, G. M. Ter-Akopian, Yu. Ts. Oganessian, A. V. Daniel, W. C. Ma, P. G. Varmette, J. O. Rasmussen, S. J. Asztalos, S. Y. Chu, K. E. Gregorich, A. O. Macchiavelly, R. W. Macleod, J. D. Cole, R. Aryaeinjad, K. Butler-Moore, M. W. Drigest, M. A. Stoyer, L. A. Bernstein, R. W. Longheed, K. J. Moody, S. G. Prussin, S. J. Zhu, H. C. Griffin, and R. Donangelo, Phys. Rev. C **57**, 2370 (1998).
[5] A. V. Ramayya, J. K. Hwang, J. H. Hamilton, A. Sandulescu, A. Florescu, G. M. Ter-Akopian, A. V. Daniel, Yu. Ts. Oganessian, G. S. Popeko, W. Greiner, J. D. Cole, and the GANDS95 Collaboration, Phys. Rev. Lett. **81**, 947 (1998).
[6] A. Sandulescu, F. Carstoiu, S. Misicu, A. Florescu, A. V. Ramayya, J. H. Hamilton, and W. Greiner, J. Phys. G **24**, 181 (1998).
[7] A. Sandulescu and W. Greiner, J. Phys. G **3**, L189 (1977).
[8] P. Ambruster, Rep. Prog. Phys. **62**, 465 (1999).
[9] J. K. Hwang, A. V. Ramayya, J. H. Hamilton, and the GANDS95 Collaboration (unpublished).
[10] F. Ajzenberg-Selove, Nucl. Phys. **A490**, 1 (1988).
[11] B. Burggraf, K. Farzin, J. Grabis, Th. Last, E. Manthey, H. P. Trautvetter, and C. Rolfs, J. Phys. G **25**, L71 (1999).
[12] A. Sandulescu, F. Carstoiu, I. Bulboaca, and W. Greiner, Phys. Rev. C **60**, 044613 (1999).
[13] G. Bertsch, J. Borysowicz, H. McManus, and W. G. Love, Nucl. Phys. **A284**, 399 (1977).
[14] G. R. Satchler and W. G. Love, Phys. Rep. **55**, 183 (1979).
[15] F. Carstoiu and R. J. Lombard, Ann. Phys. (N.Y.) **217**, 279 (1992).
[16] E. Uegaki, Prog. Theor. Phys. Suppl. **132**, 135 (1998).
[17] M. Brack, J. Damgaard, A. S. Jensen, H. C. Pauli, V. M. Strutinsky, and C. Y. Wong, Rev. Mod. Phys. **44**, 320 (1972).
[18] P. Möller, J. R. Nix, W. D. Myers, and W. J. Swiatecki, At. Data Nucl. Data Tables **59**, 185 (1995).
[19] P. Heeg, Ph.D. thesis, T. H. Darmstadt, 1990.
[20] S. Misicu, A. Sandulescu, F. Carstoiu, M. Rizea, and W. Greiner, Nuovo Cimento A **112**, 300 (1999).